SCIENCE CHINA
Technological Sciences

•Article•

https://doi.org/10.1007/s11431-018-9305-5

Modelling three dimensional dynamic problems using the four-node tetrahedral element with continuous nodal stress

ZHANG GuoHua & YANG YongTao*

State Key Laboratory of Geomechanics and Geotechnical Engineering, Institute of Rock and Soil Mechanics, Chinese Academy of Sciences, Wuhan 430071, China

Received March 1, 2018; accepted June 8, 2018; published online October 18, 2018

A partition of unity (PU) based four-node tetrahedral element with continuous nodal stress (Tetr4-CNS) was recently proposed for static analysis of three-dimensional solids. By simply using the same mesh as the classical four-node tetrahedral (Tetr4) element, high order global approximation function in the Tetr4-CNS element can be easily constructed without extra nodes or nodal DOFs. In this paper, the Tetr4-CNS element is further applied in the analysis of three dimensional dynamic problems. A series of free vibration and forced vibration problems are solved using the Tetr4-CNS element. The numerical results show that, for regular meshes, accuracy obtained using the Tetr4-CNS element is superior to that obtained using the Tetr4 and eight-node hexahedral (Hexa8) elements. For distorted meshes, the Tetr4-CNS element has better mesh-distortion tolerance than both the Tetr4 and Hexa8 elements.

partition of unity, tetrahedral element, Tetr4-CNS, mesh distortion, dynamic problems

Citation: Zhang G H, Yang Y T. Modelling three dimensional dynamic problems using the four-node tetrahedral element with continuous nodal stress. Sci China Tech Sci, 2018, 61, https://doi.org/10.1007/s11431-018-9305-5

1 Introduction

The finite element method (FEM) [1,2] is the most widely used numerical method for the analysis of dynamic problems of structures. When using FEM, engineers prefer 2D three-node triangular (Tria3) element and 3D four-node tetrahedral (Tetr4) element to 2D four-node quadrilateral (Quad4) element and 3D eight-node hexahedral (Hexa8) element for the easy creation of meshes for 2D or 3D geometries of general complexity. Additionally, the *h*-type mesh refinement adaptation using the Tria3 and Tetr4 elements can be easily conducted without difficulty, leading to the convenience in modelling and simulation [3]. Therefore, the research on the computational methods using low order triangular or tetrahedral mesh with high accuracy and versatility is of considerable practical significance [4].

However, the Tria3 and Tetr4 elements also suffer from crucial shortcomings for problems of solid mechanics. For example, due to the adoption of linear displacement approximation function, both the Tria3 and Tetr4 elements exhibit the well-known overly-stiff behavior, which leads to large error in both static and dynamic analysis [3]. More importantly, in FEM conforming mesh has to be employed to discretize the domain of problem. In other words, Tria3 and Tetr4 elements, as two types of numerical models in FEM, also have to conform the problem boundary and fracture face. When solving fracture propagation problems, the procedure to regenerate mesh around the fracture-tip, which is normally time-consuming, has to be executed in each step. For the purpose of alleviating these shortcomings, many efforts have been made in the past years [5–9].

On the other hand, meshfree methods [10–14] offer attractive alternatives to the FEM for various types of problems. The meshfree methods are very suitable for crack

* Corresponding author (email: scuhhc@126.com)

propagation problems [15], because they use a series of nodes instead of mesh to discretize the problem domain. In addition, due to the adoption of high order global approximation function, accuracy obtained using meshfree methods is generally better than that obtained using the FEM. However, meshfree methods are also not free from drawbacks. One is the lack of Kronecker-delta property for some of the meshfree methods. The other is high computational cost in obtaining shape functions [16]. Alternatively, a series of partition-of-unity (PU) based methods have been proposed in recent years to overcome the difficulties encountered in the FEM, including the extended finite element method (XFEM) [17], the generalized finite element method (GFEM) [18], the numerical manifold method (NMM) [19–35] and the isogeometric analysis [36,37].

By using the Tria3 mesh, a partition of unity (PU) based "FE-Meshfree" three-node triangular element with continuous nodal stress (Tria3-CNS) [38] was proposed recently. In the Tria3-CNS element, high order global approximation can be easily constructed without extra nodes or nodal DOFs. More importantly, the "linear dependence" (LD) issue [39], which cripples some of the PU-based methods, does not exist in this Tria3-CNS element. It has been found that Tria3-CNS element can obtain much better accuracy and higher convergence rate than both Tria3 and Quad4 elements for static and dynamic problems [38,40]. By incorporating advantages of NMM, the Tria3-CNS element is able to solve crack problems with very high accuracy [41].

Note that only a few practical engineering problems can be simplified into 2D problems. Therefore, developing effective numerical methods which can accurately simulate 3D problems is essential [5]. Since the Tetr4 element cannot obtain desirable accuracy for many engineering problems, but has great advantages in terms of mesh creation and *h*-type mesh refinement adaptation, there is a natural demand in developing a new element, which can yield high accuracy by using the same mesh as the Tetr4 element.

Recently, a PU-based four-node tetrahedral element with continuous nodal stress (Tetr4-CNS) [42] was developed. By simply using the same mesh as the Tetr4 element, high order global approximation function can be constructed in the Tetr4-CNS element without extra nodes or nodal DOFs, thereby achieving higher accuracy and convergence rate for linear elastic problems in 3D. This Tetr4-CNS element deserves to be further applied in the analysis of other types of three dimensional problems, such as dynamic problems which will be considered in this study, and crack propagation problems, which will be considered in our future work.

2 Shape function for Tetr4-CNS element

The procedure to construct shape functions of the Tetr4-CNS element has been presented in detail in ref. [42]. Hence, only the basic expressions are reviewed in this section.

Let a tetrahedral element defined by four nodes $\{P_1\ P_2\ P_3\ P_4\}$ and introduce an arbitrary point $P(\mathbf{x})$. Here, $\mathbf{x}=(x, y, z)$. As a PU-based method, the global approximation function $u^h(\mathrm{x})$ of Tera4-CNS element can be expressed as

$$u^h(\mathbf{x}) = \sum_{i=1}^{4} w_i(\mathbf{x}) u_i(\mathbf{x}), \tag{1}$$

where $w_i(\mathbf{x})$ and $u_i(\mathbf{x})$ are the weight function and local approximation function associated with node i, respectively.

The coordinate transformation for a given point is expressed as [1]

$$x = \sum_{i=1}^{4} \widetilde{N}_i(\xi, \eta, \zeta) x_i, \tag{2a}$$

$$y = \sum_{i=1}^{4} \widetilde{N}_i(\xi, \eta, \zeta) y_i, \tag{2b}$$

$$z = \sum_{i=1}^{4} \widetilde{N}_i(\xi, \eta, \zeta) z_i, \tag{2c}$$

where $\widetilde{N}_i$ are expressed in the following form:

$$\widetilde{N}_1 = 1 - \xi - \eta - \zeta, \tag{3a}$$

$$\widetilde{N}_2 = \xi, \tag{3b}$$

$$\widetilde{N}_3 = \eta, \tag{3c}$$

$$\widetilde{N}_4 = \zeta. \tag{3d}$$

In the Tera4-CNS element, weight functions $\{w_i(\mathbf{x}), i=1, 2, ..., 4\}$ are constructed by using volume coordinates and expressed as [42]

$$w_i = L_i + L_i L_i L_j + L_i L_i L_k + L_i L_i L_m - L_i L_j L_j - L_i L_k L_k - L_i L_m L_m, \tag{4}$$

where subscript i varies from 1 to 4, and j, k and m are determined by cyclic permutation of the order of i, j, k and m. Note that weight functions of the Tera4-CNS element have four important features, which can be found in Appendix A.

The local approximation function associated with node i is expressed in the interpolation form as

$$u_i(\mathbf{x}) = \sum_{j=1}^{n^{[i]}} \hat{\phi}_j^{[i]}(\mathbf{x}) a_j, \tag{5}$$

where $n^{[i]}$ is the total number of nodes in domain Ω_i (see Figure B1), a_j is the nodal displacement of node j and $\hat{\phi}_j^{[i]}$ is the shape function corresponding to $u_i(\mathbf{x})$ (The procedure to obtain u_i is described in Appendix B).

Substituting eqs. (4) and (5) into eq. (1), then the global approximation function for the Tetr4-CNS element is expressed as

$$u^h(\mathbf{x}) = \sum_{i=1}^{4} w_i(\mathbf{x}) \sum_{j=1}^{n^{[i]}} \hat{\phi}_j^{[i]}(\mathbf{x}) a_j. \tag{6}$$

By manipulating eq. (6), $u^h(\mathbf{x})$ can be expressed in a simper form as

$$u^h(\mathbf{x}) = \sum_{i=1}^{N} \phi_i(\mathbf{x}) a_i, \tag{7}$$

where $\phi_i(\mathbf{x})$ is the shape function corresponding to node i. N is the total number of nodes in the element support domain $\widehat{\Omega}$ (Definition of $\widehat{\Omega}$ can be found in Appendix B).

There are two useful properties for the Tera4-CNS element including, (1) the derivatives of $u^h(\mathbf{x})$ are continuous at the nodes; (2) the Kronecker-delta property

$$\phi_i(\mathbf{x}_j) = \delta_{ij}. \tag{8}$$

Shape functions of the Tetr4-CNS element possess the Kronecker-delta property, which is very important to impose the essential boundary conditions directly. However, due to the adoption of high order global approximate function, applying the boundary conditions only at the boundary nodes may not sufficient. This is a demerit of the Tetr4-CNS element. Note that this demerit also exists in other types of elements [43,44] which have been successfully used to solve solid problems. Similar to those elements [43,44], no ill-effect has been found in the Tetr4-CNS element.

3 Tetr4-CNS element for dynamic analysis

Consider a three dimensional problem domain defined with V and let V be discretized by a set of non-overlapping tetrahedral elements. V can therefore be express as $V = \cup_{i=1}^{N} V_i$. Here, V_i represents the domain of the i-th tetrahedral element. Using shape functions of the Tetr4-CNS element (eq. (7)), the discretized equation system for dynamic analysis can be expressed with eq. (9) [45,46].

$$\mathbf{M}\ddot{\mathbf{a}} + \mathbf{C}\dot{\mathbf{a}} + \mathbf{K}\mathbf{a} = \mathbf{f}, \tag{9}$$

where $\mathbf{K}$ denotes the global stiffness matrix; $\mathbf{M}$ represents the global mass matrix. $\mathbf{K}$ and $\mathbf{M}$ can separately be obtained by summing all the element stiffness matrices and mass matrices:

$$\mathbf{K}_{ij} = \sum \mathbf{K}_{ij}^{e}, \mathbf{M}_{ij} = \sum \mathbf{M}_{ij}^{e}, \tag{10}$$

where

$$\mathbf{K}_{ij}^{e} = \int_{V_k} \mathbf{B}_i^{\mathrm{T}} \mathbf{D} \mathbf{B}_j \mathrm{d}\Omega, \tag{11}$$

$$\mathbf{M}_{ij}^{e} = \int_{V_k} \rho \boldsymbol{\varphi}_i^{\mathrm{T}} \boldsymbol{\varphi}_j \mathrm{d}\Omega, \tag{12}$$

$$\mathbf{B}_i = \begin{bmatrix} \frac{\partial \phi_i}{\partial x} & 0 & 0 \\ 0 & \frac{\partial \phi_i}{\partial y} & 0 \\ 0 & 0 & \frac{\partial \phi_i}{\partial z} \\ \frac{\partial \phi_i}{\partial y} & \frac{\partial \phi_i}{\partial x} & 0 \\ 0 & \frac{\partial \phi_i}{\partial z} & \frac{\partial \phi_i}{\partial y} \\ \frac{\partial \phi_i}{\partial z} & 0 & \frac{\partial \phi_i}{\partial x} \end{bmatrix}, \tag{13}$$

$$\boldsymbol{\varphi}_i = \begin{bmatrix} \varphi_i & 0 & 0 \\ 0 & \varphi_i & 0 \\ 0 & 0 & \varphi_i \end{bmatrix}^{\mathrm{T}}, \tag{14}$$

and $\mathbf{D}$ in eq. (11) is the elastic matrix. Note that in eqs. (13) and (14), ϕ_i is constructed using the same method presented in eq. (7). To be more specifically, the element stiffness matrix and element mass matrix for the proposed Tetr4-CNS element have equal dimensions, which are both larger than those for the traditional FEM Tetr4 element.

In this study, the Rayleigh damping [1] is used. Hence, the damping matrix $\mathbf{C}$ is obtained through a linear combination of $\mathbf{K}$ and $\mathbf{M}$:

$$\mathbf{C} = \beta_1 \mathbf{M} + \beta_2 \mathbf{K}, \tag{15}$$

where β_1 and β_2 are the Rayleigh damping coefficients.

To solve the system equations (eq. (9)), the Newmark method [1] is employed. Assuming the state variables at time t is known, then the new state variables at time $t+\Delta t$ can be obtained using the following expressions:

$$\left(\mathbf{K} + \frac{1}{\alpha \Delta t^2}\mathbf{M} + \frac{\delta}{\alpha \Delta t}\mathbf{C}\right)\mathbf{a}_{t+\Delta t} =$$

$$\mathbf{f}_{t+\Delta t} + \mathbf{M}\left[\frac{1}{\alpha \Delta t^2}\mathbf{a}_t + \frac{1}{\alpha \Delta t}\dot{\mathbf{a}}_t + \left(\frac{1}{2\alpha} - 1\right)\ddot{\mathbf{a}}_t\right] \tag{16}$$

$$+\mathbf{C}\left[\frac{\delta}{\alpha \Delta t}\mathbf{a}_t + \left(\frac{\delta}{\alpha} - 1\right)\dot{\mathbf{a}}_t + \left(\frac{\delta}{2\alpha} - 1\right)\Delta t\left(\frac{1}{2\alpha} - 1\right)\ddot{\mathbf{a}}_t\right],$$

$$\ddot{\mathbf{a}}_{t+\Delta t} = \frac{1}{\alpha \Delta t^2}(\mathbf{a}_{t+\Delta t} - \mathbf{a}_t) - \frac{1}{\alpha \Delta t}\dot{\mathbf{a}}_t - \left(\frac{1}{2\alpha} - 1\right)\ddot{\mathbf{a}}_t, \tag{17}$$

$$\dot{\mathbf{a}}_{t+\Delta t} = \dot{\mathbf{a}}_t + \Delta t(1-\delta)\ddot{\mathbf{a}}_t + \delta \Delta t \ddot{\mathbf{a}}_{t+\Delta t}. \tag{18}$$

By neglecting the damping and forcing terms, eq. (9) can be simplified into a homogenous equation:

$$\mathbf{M}\ddot{\mathbf{a}} + \mathbf{K}\mathbf{a} = 0. \tag{19}$$

A general solution of eq. (19) can be written as

$$\mathbf{a} = \bar{\mathbf{a}} \exp(i\omega t), \tag{20}$$

where t denotes time. $\bar{\mathbf{a}}$ is the eigenvector and ω is the natural frequency.

Substituting eq. (20) into eq. (19), then the natural frequency ω can be obtained by solving the following eigenvalue equation:

$$\mathbf{K}\bar{\mathbf{a}} - \lambda \mathbf{M}\bar{\mathbf{a}} = 0, \lambda = \omega^2. \tag{21}$$

Here, the eigenvectors $\bar{\mathbf{a}}$ determine the mode shapes of free vibration associated with ω. Solving all the modes of the problem will be extremely time-consuming. As a result, generally, only those lower order modes with smaller ω are seek out by using, for instance, the subspace iteration procedure [1].

4 Numerical examples

To assess performance of the Tetr4-CNS model for structural dynamic problems, four numerical tests for free vibration

problems and one numerical test for forced vibration problem are solved. Except specially mentioned, physical units used in this section are based on the international standard unit system. Here, n represents the total number of nodes in the computational model. To assess accuracy, the relative error in the natural frequency is defined as

$$Re = \frac{\omega^{num} - \omega^{\mathrm{ref}}}{\omega^{\mathrm{ref}}}, \tag{22}$$

where the "ref" represents a reference solution and the "num" denotes a numerical solution.

The numerical models used in this section are listed as follows:

(1) Tetr4 element: four-node isoparametric tetrahedral element;

(2) Hexa8 element: eight-node isoparametric hexahedral element;

(3) Tetr10 element: ten-node isoparametric tetrahedral element;

(4) Hexa20 element: twenty-node isoparametric hexahedral element;

(5) Tetr4-CNS (LS10) element: the first type of Tetr4-CNS element, which uses the basis from eq. (A7) to construct local approximation functions;

(6) Tetr4-CNS (LS20) element: the second type of Tetr4-CNS element, which employs the basis from eq. (A8) to construct local approximation functions.

4.1 Mesh distortion test

To investigate performance of the Tetr4-CNS element for distorted meshes, a 3D straight cantilever beam is employed. As shown in Figure 1, the 3D straight cantilever beam is discretized into 2×2×2 elements to investigate the performance of Hexa8 and Hexa20 elements. In addition, the hexahedral meshes shown in Figure 1 are further divided into tetrahedral meshes to assess the performance of Tetr4, Tetr10, Tetr4-CNS (LS10) and Tetr4-CNS (LS20) elements. As can be seen from Figure 2, each hexahedral element is divided into 6 tetrahedral elements.

In this study, we consider two types of distortion, namely, the plain-distorted and skewed-distorted elements. In the computation, a distortion parameter $2d/W$ is used to control mesh distortion. When considering plane-distorted elements, nodes A, B, C, G, H and I are moved longitudinally, by a distance $\pm d$ to induce distortion. When considering skewed-distorted elements, node E is moved longitudinally by a distance. Note that this example has already been used to evaluate the performance of Tetr4-CNS (LS10) and Tetr4-CNS (LS20) elements in solving static problems [42].

In this example, the left end of the beam is fixed. The parameters used are taken as: L=10, H=2, W=2, Young's modulus E=1500, Poisson's ratio v=0.25 and mass density ρ=1. The reference solution of the fundamental natural frequency for this cantilever beam is 0.1222, which is obtained by ABAQUS with a very fine mesh with 320000 Hexa8 elements and 337881 nodes. Comparisons of computed natural frequency of the first mode through the plane-distorted and skewed-distorted elements are separately shown in Tables 1 and 2. The comparisons of relative errors obtained by using different element types are shown in Figure 3. Some conclusions can be drawn:

(1) First, the errors given by Tetr4-CNS (LS10) and Tetr4-CNS (LS20) elements almost do not change with the increase in distortion parameters, while the errors given by Tetr4 and Hexa8 elements show a rapid increase. The Tetr4-CNS (LS10) and Tetr4-CNS (LS20) elements are seen to be insensitive to mesh distortion.

(2) Second, the results of Tetr4-CNS (LS10) element are always much better than those of Tetr4 and Hexa8 elements. The results of Tetr4-CNS (LS20) element is slightly better than those of Tetr4-CNS (LS10) element.

(3) Third, accuracy obtained using the Tetr10 and Hexa20 elements are even better than those obtained using the Tetr4-CNS (LS20) element. However, as the value of distortion parameter increases, the results obtained by using the Tetr10 and Hexa20 elements deteriorate. Additionally, both Tetr10 and Hexa20 elements need adding extra nodes, resulting in a fast expanding global stiffness and mass matrices.

It is known that certain elements are sensitive to certain types of distortions, i.e. linear elements fear linear distortions (angular distortion) while high order elements are immune to linear (angular) distortion [47,48]. As shape functions of the Tetr4-CNS (LS10) and Tetr4-CNS (LS20) elements are not linear, they are hence immune to linear distortions tested in

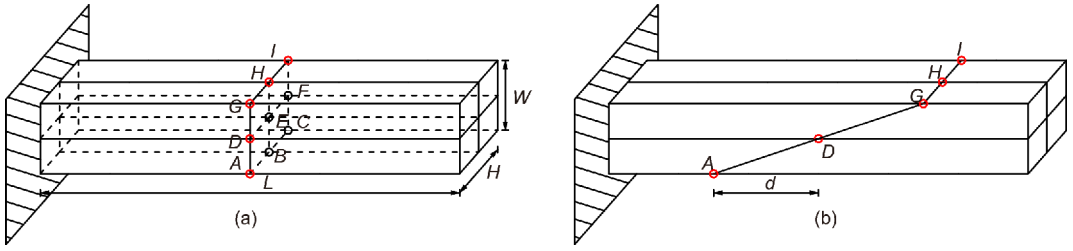

Figure 1 (Color online) Straight cantilever beam for distortion test [43]. (a) Regular hexahedral mesh; (b) distorted hexahedral mesh generated by longitudinally shifting the associated nodes by a distance d.

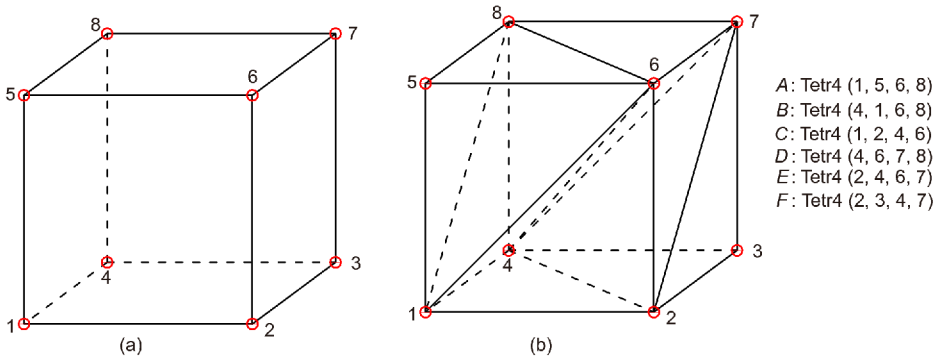

Figure 2 (Color online) Sketch of dividing a Hexa8 element into six Tetr4 elements. (a) A Hexa8 element; (b) six Tetr4 elements.

Table 1 Computed natural frequencies (Hz) of the first mode through the plane-distorted elements

$2d/W$	Tetr4	Hexa8	Tetr10	Hexa20	Tetr4-CNS (LS10)	Tetr4-CNS (LS20)	Reference
0.000	0.2963	0.2258	0.1277	0.1226	0.1506	0.1446	0.1222
0.025	0.2971	0.2259	0.1277	0.1227	0.1506	0.1446	0.1222
0.050	0.2982	0.2263	0.1278	0.1227	0.1506	0.1446	0.1222
0.075	0.2995	0.2270	0.1278	0.1228	0.1507	0.1446	0.1222
0.100	0.3011	0.2279	0.1279	0.1228	0.1507	0.1446	0.1222
0.150	0.3045	0.2304	0.1281	0.1231	0.1507	0.1446	0.1222
0.200	0.3082	0.2336	0.1284	0.1235	0.1507	0.1446	0.1222
0.250	0.3119	0.2371	0.1288	0.1240	0.1508	0.1446	0.1222
0.300	0.3156	0.2408	0.1293	0.1245	0.1508	0.1446	0.1222
0.400	0.3226	0.2481	0.1306	0.1260	0.1509	0.1446	0.1222
0.500	0.3290	0.2546	0.1323	0.1276	0.1510	0.1446	0.1222
0.600	0.3348	0.2604	0.1342	0.1294	0.1511	0.1446	0.1222
0.700	0.3403	0.2654	0.1361	0.1309	0.1512	0.1445	0.1222
0.800	0.3456	0.2699	0.1379	0.1323	0.1514	0.1445	0.1222
0.900	0.3507	0.2740	0.1394	0.1338	0.1515	0.1444	0.1222

this example.

4.2 A 3D cantilever beam

A three dimensional cantilever beam shown in Figure 4 and fixed at the left end is studied for the various behaviors of Tetr4-CNS element as a benchmark problem. The parameters in the computation are taken as L=4, H=1, W=0.4, Young's modulus E=71×10^9, Poisson's ratio v=0.3 and mass density ρ=2700. This problem has earlier been analyzed by He et al. [3] using an edge-based smoothed tetrahedron finite element method (ES-T-FEM). Due to the lack of analytical solution for this problem, a reference solution is obtained by He et al. [3] using Nastran with a very fine mesh of 18241 nodes for comparison purpose.

To examine the convergence of numerical solution in Tetr4, Hexa8, Tetr4-CNS (LS10) and Tetr4-CNS (LS20) elements, three discrete models are constructed, as shown in Figures 5 and 6. The first 6 non-rigid eigenfrequencies of the 3D beam obtained from Tetr4-CNS (LS10) and Tetr4-CNS (LS20) elements are listed in Tables 3–5, together with the numerical solutions obtained using the Tetr4 element with the same set of mesh. In addition, results obtained using the Hexa8 element with hexahedral mesh are also provided in Tables 3–5. Figure 7 shows the plot of errors in the first two natural frequencies obtained using the Tetr4-CNS (LS10) and Tetr4-CNS (LS20) elements as well as the Tetr4 and Hexa8 elements. It is seen that errors in the first two natural frequencies given by Tetr4-CNS (LS10) element is generally less than that given by the Tetr4 and Hexa8 elements. Additionally, Tetr4-CNS (LS20) element can obtain even better results than Tetr4-CNS (LS10) element. Even for coarse mesh, results given by the Tetr4-CNS (LS20) element are close to the reference solution.

The eigenmodes of Modes 5, 10 and 15 obtained by using the Tetr4 and Tetr4-CNS (LS20) element are separately

Table 2 Computed natural frequencies (Hz) of the first mode through the skewed-distorted elements

2*d*/*W*	Tetr4	Hexa8	Tetr10	Hexa20	Tetr4-CNS (LS10)	Tetr4-CNS (LS20)	Reference
0.000	0.2963	0.2258	0.1277	0.1226	0.1506	0.1446	0.1222
0.025	0.2976	0.2269	0.1277	0.1227	0.1506	0.1446	0.1222
0.050	0.2995	0.2284	0.1277	0.1227	0.1506	0.1446	0.1222
0.075	0.3018	0.2302	0.1277	0.1227	0.1506	0.1446	0.1222
0.100	0.3044	0.2323	0.1278	0.1227	0.1506	0.1446	0.1222
0.150	0.3098	0.2370	0.1279	0.1228	0.1506	0.1446	0.1222
0.200	0.3150	0.2422	0.1281	0.1229	0.1506	0.1446	0.1222
0.250	0.3194	0.2473	0.1283	0.1230	0.1506	0.1446	0.1222
0.300	0.3232	0.2522	0.1286	0.1232	0.1506	0.1446	0.1222
0.400	0.3290	0.2605	0.1296	0.1238	0.1506	0.1446	0.1222
0.500	0.3332	0.2668	0.1310	0.1246	0.1506	0.1446	0.1222
0.600	0.3365	0.2715	0.1328	0.1255	0.1507	0.1446	0.1222
0.700	0.3394	0.2749	0.1347	0.1267	0.1507	0.1445	0.1222
0.800	0.3419	0.2777	0.1365	0.1281	0.1507	0.1445	0.1222
0.900	0.3443	0.2799	0.1382	0.1296	0.1507	0.1445	0.1222

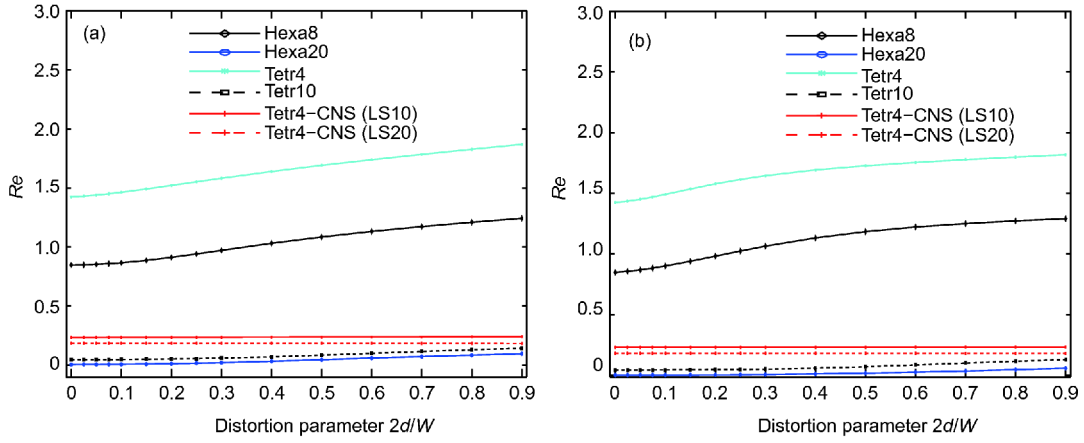

Figure 3 (Color online) Errors in the computed frequencies of the first mode for distortion sensitivity test. (a) Plane-distorted elements; (b) skewed-distorted elements.

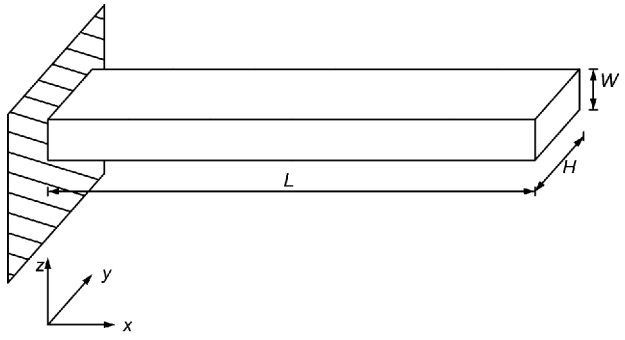

Figure 4 Free vibration analysis of a 3D cantilever beam.

plotted in Figures 8 and 9. It can be observed that the computed eigenmodes from Tetr4-CNS (LS20) element are similar to those from Tetr4 element and no spurious modes exist.

4.3 A 3D lame problem

In this section, a 3D Lame problem which consists of a hollow sphere is considered. Due to the symmetry, only one-eighth of the hollow sphere is modeled, as shown in Figure 10. The parameters for this problem are listed as: inner radius of the hollow sphere a=1 m, outer radius of the hollow sphere b=2 m, Young's modulus E=1000 N m^{-2}, Poisson's ratio v=0.3 and mass density ρ=1 kg m^{-3}. Due to the lack of analytical solution, a reference solution is obtained by using the Tetr10 element with a very fine mesh of 18593 nodes for comparison purpose.

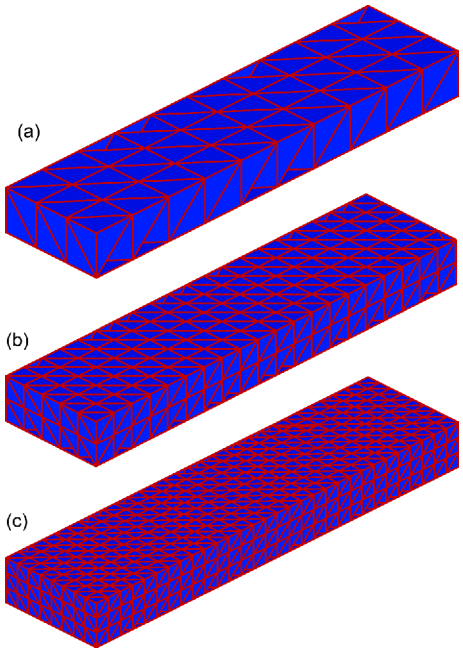

Figure 5 (Color online) Regular tetrahedral mesh for the 3D cantilever beam in Figure 4. (a) Mesh A (88 nodes, 180 elements); (b) Mesh B (378 nodes, 1200 elements); (c) Mesh C (1116 nodes, 4320 elements).

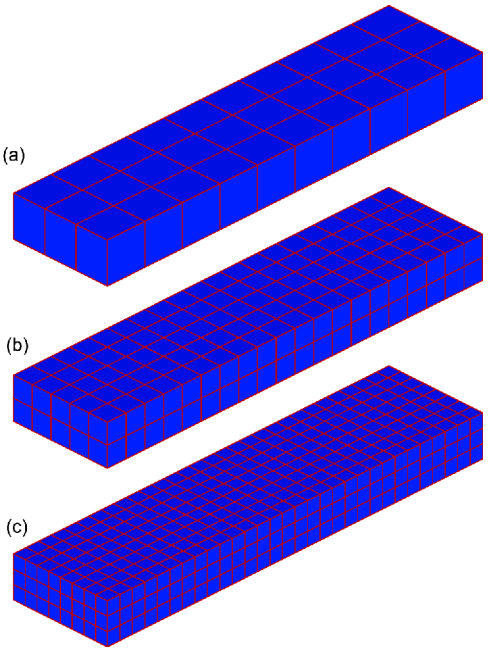

Figure 6 (Color online) Regular hexahedral mesh for the 3D cantilever beam in Figure 4. (a) Mesh A (88 nodes, 30 elements); (b) Mesh B (378 nodes, 200 elements); (c) Mesh C (1116 nodes, 720 elements).

Table 3 Comparison of computed frequencies (Hz) for the 3D cantilever beam using Mesh A (Figures 5(a) and 6(a))

Mode	Tetr4 (88 nodes, 180 elements)	Hexa8 (88 nodes, 30 elements)	Tetr4-CNS (LS10) (88 nodes, 180 elements)	Tetr4-CNS (LS20) (88 nodes, 180 elements)	Ref. [3]
1	48.44	25.69	22.96	22.24	20.77
2	63.48	52.25	50.70	50.54	49.72
3	261.52	140.64	146.48	140.37	124.47
4	309.13	155.78	154.43	140.76	132.45
5	326.98	268.94	264.45	259.89	252.26
6	374.68	324.24	323.90	323.50	321.94

Table 4 Comparison of computed frequencies (Hz) for the 3D cantilever beam using Mesh B (Figures 5(b) and 6(b))

Mode	Tetr4 (378 nodes, 1200 elements)	Hexa8 (378 nodes, 200 elements)	Tetr4-CNS (LS10) (378 nodes, 1200 elements)	Tetr4-CNS (LS20) (378 nodes, 1200 elements)	Ref. [3]
1	31.31	22.22	20.94	20.88	20.77
2	54.10	50.52	50.01	49.89	49.72
3	182.15	133.94	126.58	125.74	124.47
4	218.31	137.24	137.25	135.31	132.45
5	271.80	257.44	253.79	252.81	252.26
6	323.71	322.78	322.55	322.36	321.94

To examine convergence of numerical solution in the Tetr4, Tetr4-CNS (LS10) and Tetr4-CNS (LS20) elements, three discrete models are used. The first 6 non-rigid eigenfrequencies of the one-eighth of the hollow sphere obtained using the Tetr4-CNS (LS10) and Tetr4-CNS (LS20) elements are listed in Tables 6–8, together with the numerical solutions obtained using the Tetr4 element with the same set of meshes. Figure 11 shows the plot of errors in the first two natural frequencies obtained using the Tetr4-CNS (LS10), Tetr4-CNS (LS20) and Tetr4 elements. It is seen that errors in the first two natural frequencies given by the Tetr4-CNS (LS10) element is much less than that given by the Tetr4

Table 5 Comparison of computed frequencies (Hz) for the 3D cantilever beam using Mesh C (Figures 5(c) and 6(c))

Mode	Tetr4 (1116 nodes, 4320 elements)	Hexa8 (1116 nodes, 720 elements)	Tetr4-CNS (LS10) (1116 nodes, 4320 elements)	Tetr4-CNS (LS20) (1116 nodes, 4320 elements)	Ref. [3]
1	26.45	21.44	20.86	20.82	20.77
2	51.63	50.10	49.86	49.81	49.72
3	156.23	128.88	125.25	124.90	124.47
4	181.24	134.77	133.83	133.07	132.45
5	260.92	254.65	252.89	252.51	252.26
6	322.95	322.40	322.28	322.18	321.94

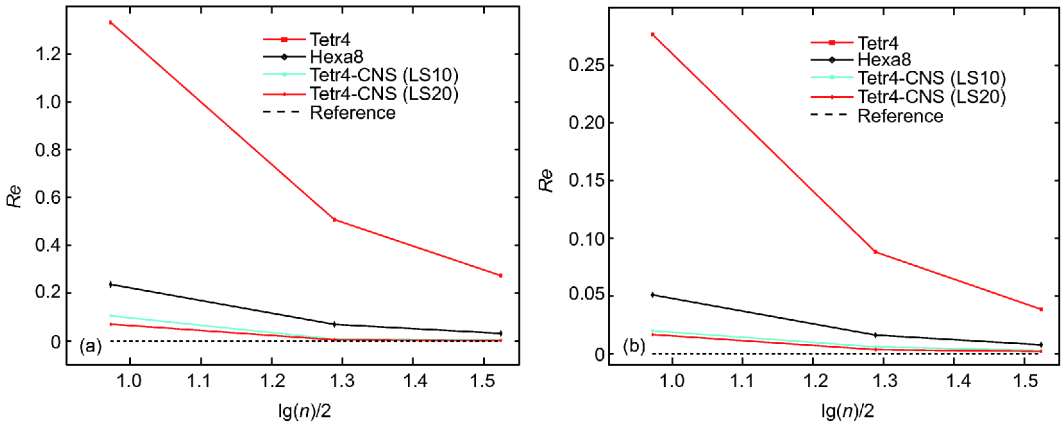

Figure 7 (Color online) Convergence of the error in the computed frequency for the first two modes for the 3D cantilever beam. (a) Mode 1; (b) Mode 2.

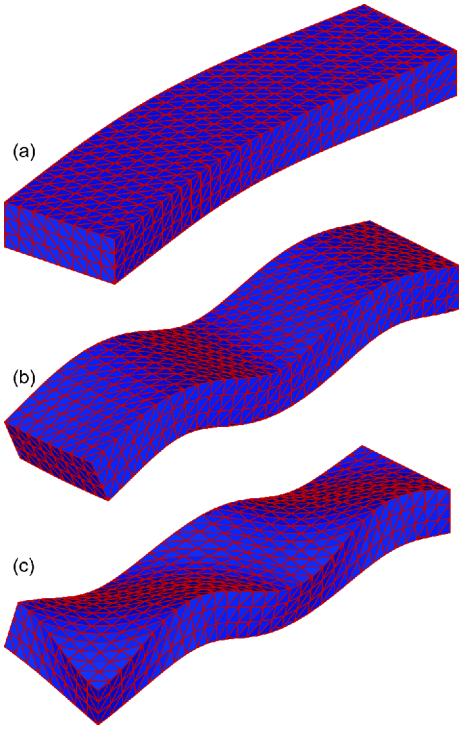

Figure 8 (Color online) Eigenmodes of 3D cantilever beam problem obtained by using the Tetr4 element. (a) Mode 5; (b) Mode 10; (c) Mode 15.

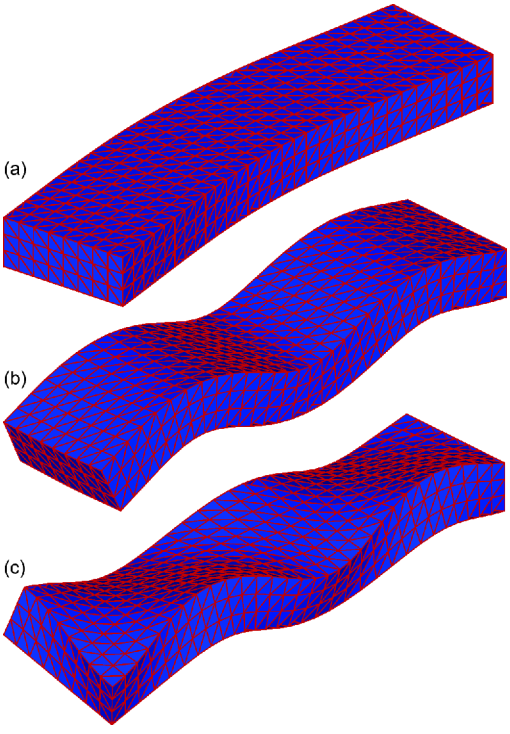

Figure 9 (Color online) Eigenmodes of 3D cantilever beam problem obtained by using the Tetr4-CNS (LS20) element. (a) Mode 5; (b) Mode 10; (c) Mode 15.

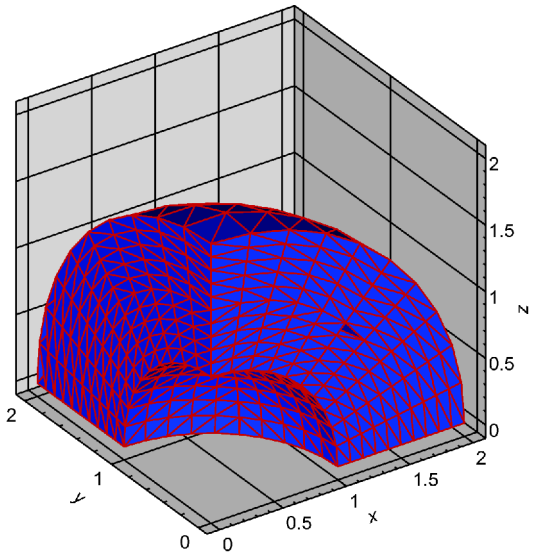

Figure 10 (Color online) One-eighth of a hollow sphere model discretized using four-node tetrahedral elements [42].

Table 6 Comparison of computed frequencies (Hz) for the one-eighth of the hollow sphere using Model A (259 nodes, 972 elements)

Mode	Tetr4	Tetr4-CNS (LS10)	Tetr4-CNS (LS20)	Reference
1	8.74	8.24	7.96	7.63
2	9.03	8.28	8.09	7.92
3	9.59	8.30	8.09	7.93
4	12.12	10.88	10.34	10.11
5	12.88	11.56	10.87	10.25
6	13.52	11.74	10.90	10.29

Table 7 Comparison of computed frequencies (Hz) for the one-eighth of the hollow sphere using Model B (549 nodes, 2304 elements)

Mode	Tetr4	Tetr4-CNS (LS10)	Tetr4-CNS (LS20)	Reference
1	8.44	7.96	7.78	7.63
2	8.57	8.08	8.01	7.92
3	8.83	8.09	8.01	7.93
4	11.29	10.39	10.21	10.11
5	11.90	10.86	10.52	10.25
6	12.24	10.92	10.53	10.29

element. Additionally, Tetr4-CNS (LS20) element can obtain even better results than Tetr4-CNS (LS10) element.

4.4 A three dimensional rock slope

A three dimensional rock slope shown in Figure 12 is considered in this section. The bottom surface, left surface, right surface, front surface and back surface of the rock slope are all constrained in normal direction. Computational parameters for the rock slope are listed as follows: Young's modulus E=19 GPa, Poisson's ratio ν=0.25 and mass density ρ=2630 kg m^{-3}. Since the analytical solution for this problem is not available, a reference solution is obtained by using a very fine mesh (Figure 13) with ABAQUS.

Table 8 Comparison of computed frequencies (Hz) for the one-eighth of the hollow sphere using Model C (1001 nodes, 4500 elements)

Mode	Tetr4	Tetr4-CNS (LS10)	Tetr4-CNS (LS20)	Reference
1	8.29	7.81	7.72	7.63
2	8.34	8.01	7.98	7.92
3	8.48	8.02	7.98	7.93
4	10.89	10.23	10.16	10.11
5	11.40	10.58	10.40	10.25
6	11.63	10.62	10.40	10.29

The first 5 natural frequencies for the discretized models (Figure 12) calculated using the Hexa8, Hexa20, Hexa20, Tetr10 and Tetr4-CNS (LS20) elements are listed together in Table 9. As seen in Table 9, results obtained using the Tetr4-CNS (LS20) element are much better than those obtained using the Hexa8 element, but inferior to those obtained using the Hexa20 and Tetr10 elements.

4.5 A 3D cantilever beam subjected to a harmonic loading

The three dimensional cantilever beam presented in Section 4.2 is again investigated using the Tetr4-CNS model. The cantilever beam shown in Figure 14 is subjected to a harmonic loading $f(t)=\sin\omega_f t$. The parameters in the computation are taken as L=4, H=1, W=0.4, Young's modulus $E=71\times10^9$, Poisson's ratio ν=0.3, mass density ρ=2700, ω_f=0.04 rad s^{-1}, the Rayleigh damping coefficients β_1=0.005, β_2=0.272 and the Newmark method parameters α=0.5, δ=1.0 A time step with Δt=1.57 s is used for time integration, while the total computational time is set to be 1200 s. The discretized models shown in Figures 5(b) and 6(b) are employed in this example. The problem is solved with four types of numerical models including the Tetr4, Hexa8, Tetr4-CNS (LS10) and Tetr4-CNS (LS20) elements. Due to the lack of theoretical solution, a reference solution is obtained by using Hexa20 element with the discretized model presented in Figure 6(b) for comparison purpose. Figure 15 shows dynamic responses of the 3D cantilever beam obtained using different types of elements. For a better view, the displacement errors predicted by the Tetr4, Hexa8, Tetr4-CNS (LS10) and Tetr4-CNS (LS20) elements are further plotted in Figure 16. It is seen that errors obtained using the Tetr4-CNS (LS10) and Tetr4-CNS (LS20) elements are very small, which are much smaller as compared to those obtained using the Tetr4 and Hexa8 elements. This shows that the

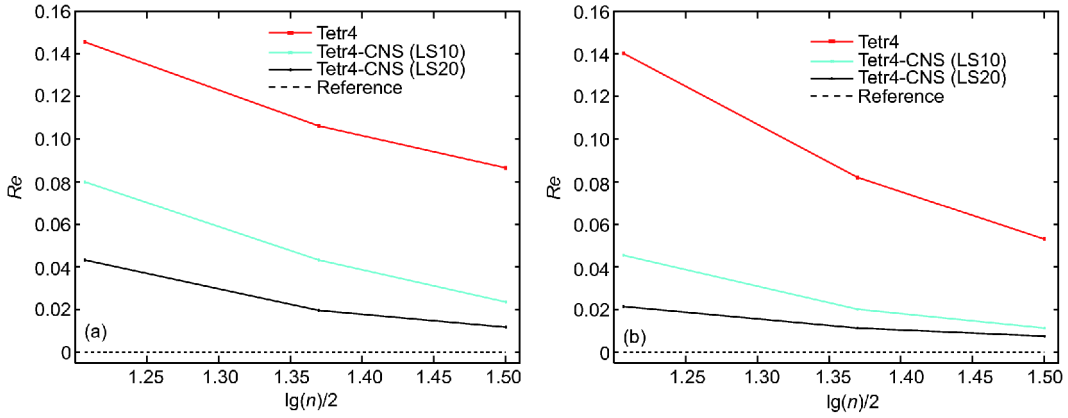

Figure 11 (Color online) Convergence of errors in the computed frequency for the first two modes of the hollow sphere. (a) Mode 1; (b) Mode 2

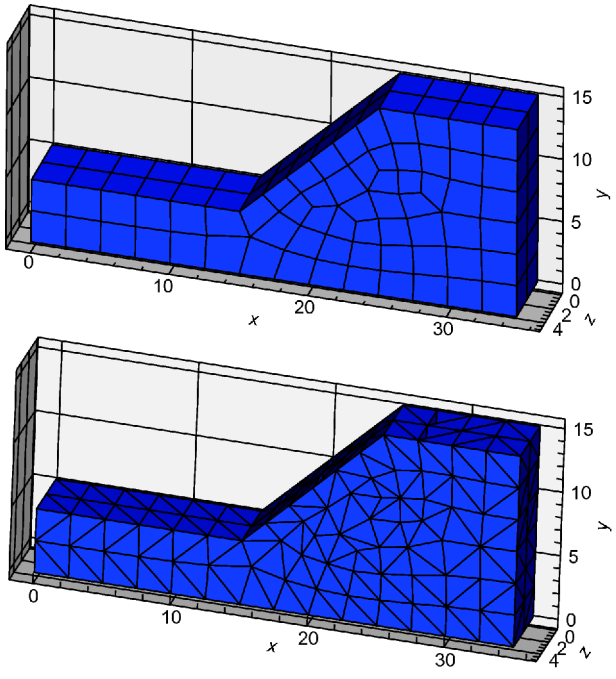

Figure 12 (Color online) Discritized model for a rock slope. (a) Hexahedral mesh; (b) tetrahedral mesh.

Tetr4-CNS (LS10) and Tetr4-CNS (LS20) elements using tetrahedral mesh can be applied to the forced vibration analysis with excellent accuracy.

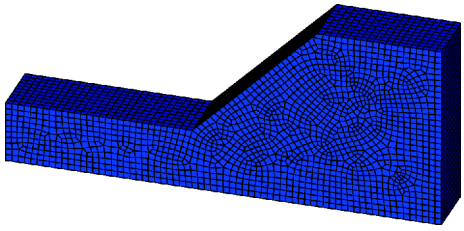

Figure 13 (Color online) A very fine mesh for the rock slope (Hexa8 element with 17666 nodes and 15110 elements).

5 Discussion and conclusions

In this paper, the PU-based four-node tetrahedral element with continuous nodal stress (Tetr4-CNS) is extended to dynamic analysis of three-dimensional solids. This Tetr4-CNS element performs very well for dynamic problems. Some important observations from this work are as follows:

(1) Compared to the FEM, Tetr4-CNS (LS10) element does not need a new mesh or additional nodes in the mesh. It just uses the same mesh as the classical Tetr4 element, but can give more accurate solution than the Tetr4 and Hexa8 elements because a higher order interpolation is used in the Tetr4-CNS (LS10) element.

(2) The Tetr4-CNS (LS20) element can obtain even better results than Tetr4-CNS (LS10) element, because the Tetr4-CNS (LS20) element employs a higher global approximation function than the Tetr4-CNS (LS10) element.

Table 9 Comparison of computed frequencies (Hz) for the rock slope

Mode	Hexa8 (246 nodes and 124 elements)	Hexa20 (839 nodes and 124 elements)	Tetr10 (1435 nodes and 744 elements)	Tetr4-CNS (LS20) (246 nodes and 744 elements)	Reference (17666 nodes and 15110 elements)
1	37.85	37.66	37.68	37.62	37.68
2	54.08	53.72	53.80	53.65	53.79
3	63.73	62.66	62.76	62.75	62.70
4	70.26	69.12	69.32	69.46	69.23
5	88.74	85.95	86.32	86.57	86.15

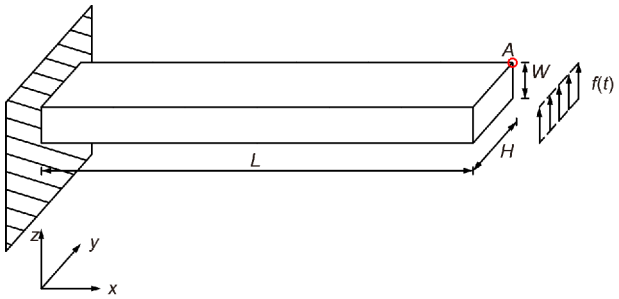

Figure 14 (Color online) A 3D cantilever beam subjected to a harmonic loading on the right end.

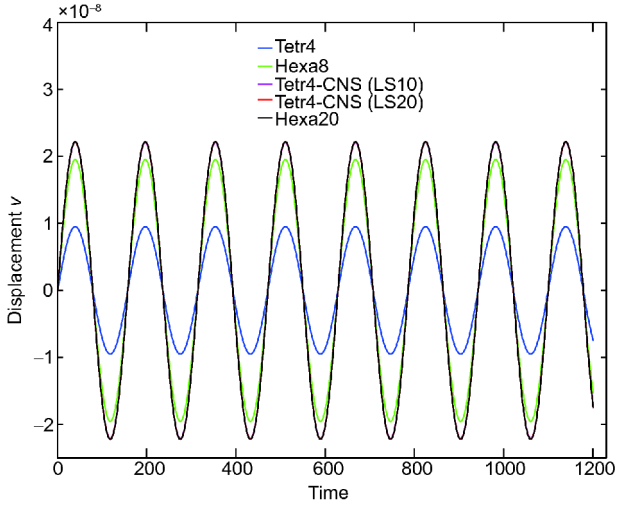

Figure 15 (Color online) Dynamic responses of a 3D cantilever beam subjected to a harmonic loading.

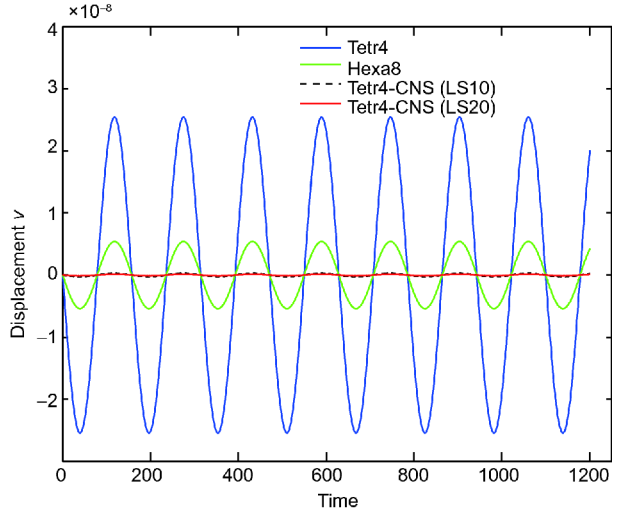

Figure 16 (Color online) Displacement errors predicted by different types of elements.

(3) Results from the mesh distortion test show that accuracy obtained using the Tetr10 and Hexa20 elements are even better than that obtained using the Tetr4-CNS (LS20) element. However, as the value of distortion parameter increases, the results obtained using the Tetr10 and Hexa20 elements deteriorate (Figure 3). Additionally, both Tetr10 and Hexa20 elements need extra nodes, resulting in a fast expanding global stiffness matrix.

Although the Tetr4-CNS (LS10) and Tetr4-CNS (LS20) elements perform better than the Tetr4 and Hexa8 elements for dynamic problems, this advantage does not come without cost. The bandwidth of the global matrix for the proposed elements is wider than that for the Tetr4 and Hexa8 elements. Hence, the time spent on solving global equations for the proposed elements is longer than that for the Tetr4 and Hexa8 elements. However, Tetr4-CNS (LS10) and Tetr4-CNS (LS20) elements demonstrate excellent distortion tolerant capability, while Tetr4 element and Hexa8 element are very sensitive to mesh quality. This advantage of the Tetr4-CNS (LS10) and Tetr4-CNS (LS20) elements is very important for practical problems, since the time spent in generating high quality mesh for problems with complex geometric boundaries is usually time consuming.

This work was supported by the National Natural Science Foundation of China (Grant Nos. 51609240, 11572009, 51538001, 51579235 & 41472288) and the National Basic Research Program of China (Grant No. 2014CB047100).

Supporting Information

The supporting information is available online at tech.scichina.com and www.springerlink.com. The supporting materials are published as submitted, without typesetting or editing. The responsibility for scientific accuracy and content remains entirely with the authors.

1 Zienkiewicz O C, Taylor R L. The Finite Element Method. 5th ed. Oxford: Butterworth-Heinemann, 2000
2 Yang Y T, Zheng H, Sivaselvan M V. A rigorous and unified mass lumping scheme for higher-order elements. Comput Methods Appl Mech Eng, 2017, 319: 491–514
3 He Z C, Li G Y, Zhong Z H, et al. An edge-based smoothed tetrahedron finite element method (ES-T-FEM) for 3D static and dynamic problems. Comput Mech, 2013, 52: 221–236
4 Liu G R. Meshfree Methods: Moving Beyond the Finite Element Method. 2nd ed. Boca Raton: CRC Press, 2009
5 Nguyen M N, Bui T Q, Truong T T, et al. Enhanced nodal gradient 3D consecutive-interpolation tetrahedral element (CTH4) for heat transfer analysis. Int J Heat Mass Transfer, 2016, 103: 14–27
6 Liu G R, Nguyen-Thoi T. Smoothed Finite Element Methods. Boca Raton: CRC Press, 2010
7 Nguyen-Thoi T, Liu G R, Vu-Do H C, et al. A face-based smoothed finite element method (FS-FEM) for visco-elastoplastic analyses of 3D solids using tetrahedral mesh. Comput Methods Appl Mech Eng, 2009, 198: 3479–3498
8 Areias P, Rabczuk T, Dias-da-Costa D. Element-wise fracture algorithm based on rotation of edges. Eng Fract Mech, 2013, 110: 113–137
9 Areias P, Rabczuk T, Camanho P P. Initially rigid cohesive laws and fracture based on edge rotations. Comput Mech, 2013, 52: 931–947
10 Zhuang X Y, Augarde C. Aspects of the use of orthogonal basis functions in the element-free Galerkin method. Int J Numer Meth Eng, 2009, 81: 366–380
11 Zhuang X, Augarde C E, Mathisen K M. Fracture modeling using meshless methods and level sets in 3D: Framework and modeling. Int

J Numer Meth Eng, 2012, 92: 969–998
12 Rabczuk T, Belytschko T, Xiao S P. Stable particle methods based on Lagrangian kernels. Comput Methods Appl Mech Eng, 2004, 193: 1035–1063
13 Liu G R, Gu Y T. A point interpolation method for two-dimensional solids. Int J Numer Meth Eng, 2001, 50: 937–951
14 Rabczuk T, Areias P M A, Belytschko T. A meshfree thin shell method for non-linear dynamic fracture. Int J Numer Meth Eng, 2007, 72: 524–548
15 Rabczuk T, Belytschko T. Cracking particles: A simplified meshfree method for arbitrary evolving cracks. Int J Numer Meth Eng, 2004, 61: 2316–2343
16 Zheng C, Wu S C, Tang X H, et al. A novel twice-interpolation finite element method for solid mechanics problems. Acta Mech Sin, 2010, 26: 265–278
17 Amiri F, Anitescu C, Arroyo M, et al. XLME interpolants, a seamless bridge between XFEM and enriched meshless methods. Comput Mech, 2014, 53: 45–57
18 Strouboulis T, Babuška I, Copps K. The design and analysis of the generalized finite element method. Comput Methods Appl Mech Eng, 2000, 181: 43–69
19 Yang Y T, Tang X H, Zheng H, et al. Three-dimensional fracture propagation with numerical manifold method. Eng Anal Bound Elem, 2016, 72: 65–77
20 Yang Y T, Zheng H. Direct approach to treatment of contact in numerical manifold method. Int J Geomech, 2017, 17: E4016012
21 Cai Y C, Zhuang X Y, Zhu H H. A generalized and efficient method for finite cover generation in the numerical manifold method. Int J Comput Method, 2013, 10: 1350028
22 Yang Y T, Xu D D, Zheng H. Evaluation on stress intensity factor of crack under dynamic load using numerical manifold method (in Chinese). Chin J Theoret Appl Mech, 2014, 46: 730–738
23 Zheng H, Xu D D. New strategies for some issues of numerical manifold method in simulation of crack propagation. Int J Numer Meth Eng, 2014, 97: 986–1010
24 Zheng H, Yang Y T. On generation of lumped mass matrices in partition of unity based methods. Int J Numer Meth Eng, 2017, 112: 1040–1069
25 Yang Y T, Xu D D, Sun G H, et al. Modeling complex crack problems using the three-node triangular element fitted to numerical manifold method with continuous nodal stress. Sci China Tech Sci, 2017, 60: 1537–1547
26 Yang Y T, Tang X H, Zheng H, et al. Hydraulic fracturing modeling using the enriched numerical manifold method. Appl Math Model, 2018, 53: 462–486
27 Yang Y T, Guo H, Fu X, et al. Boundary settings for the seismic dynamic response analysis of rock masses using the numerical manifold method. Int J Numer Anal Methods Geomech, 2018, 42: 1095–1122
28 Yang Y T, Sun G H, Zheng H, et al. A four-node quadrilateral element fitted to numerical manifold method with continuous nodal stress for crack analysis. Comput Struct, 2016, 177: 69–82
29 Wu Z J, Fan L F. The numerical manifold method for elastic wave propagation in rock with time-dependent absorbing boundary conditions. Eng Anal Bound Elem, 2014, 46: 41–50
30 Fan L F, Yi X W, Ma G W. Numerical manifold method (NMM) simulation of stress wave propagation through fractured rock. Int J Appl Mech, 2013, 05: 1350022
31 Wu Z J, Wong L N Y. Frictional crack initiation and propagation analysis using the numerical manifold method. Comput Geotech, 2012, 39: 38–53
32 Wu Z J, Wong L N Y. Elastic-plastic cracking analysis for brittle-ductile rocks using manifold method. Int J Fract, 2013, 180: 71–91
33 Wu Z J, Wong L N Y. Modeling cracking behavior of rock mass containing inclusions using the enriched numerical manifold method. Eng Geol, 2013, 162: 1–13
34 Yang Y T, Xu D D, Zheng H. Explicit discontinuous deformation analysis method with lumped mass matrix for highly discrete block system. Intern J Geomech, 2018, 18: 04018098
35 Wu Z J, Wong L N Y, Fan L F. Dynamic study on fracture problems in viscoelastic sedimentary rocks using the numerical manifold method. Rock Mech Rock Eng, 2013, 46: 1415–1427
36 Nguyen V P, Anitescu C, Bordas S P A, et al. Isogeometric analysis: An overview and computer implementation aspects. Math Comput Simul, 2015, 117: 89–116
37 Anitescu C, Jia Y, Zhang Y J, et al. An isogeometric collocation method using superconvergent points. Comput Methods Appl Mech Eng, 2015, 284: 1073–1097
38 Yang Y T, Tang X H, Zheng H. A three-node triangular element with continuous nodal stress. Comput Struct, 2014, 141: 46–58
39 Babuška I, Melenk J M. The partition of unity method. Int J Numer Meth Eng, 1997, 40: 727–758
40 Yang Y T, Xu D D, Zheng H. Application of the three-node triangular element with continuous nodal stress for free vibration analysis. Comput Struct, 2016, 169: 69–80
41 Yang Y T, Zheng H. A three-node triangular element fitted to numerical manifold method with continuous nodal stress for crack analysis. Eng Fract Mech, 2016, 162: 51–75
42 Yang Y T, Sun G H, Zheng H. A four-node tetrahedral element with continuous nodal stress. Comput Struct, 2017, 191: 180–192
43 Ooi E T, Rajendran S, Yeo J H, et al. A mesh distortion tolerant 8-node solid element based on the partition of unity method with inter-element compatibility and completeness properties. Finite Elem Anal Des, 2007, 43: 771–787
44 Xu J P, Rajendran S. A partition-of-unity based 'FE-Meshfree' QUAD4 element with radial-polynomial basis functions for static analyses. Comput Methods Appl Mech Eng, 2011, 200: 3309–3323
45 Liu G R, Gu Y T. A local radial point interpolation method (LRPIM) for free vibration analyses of 2-d solids. J Sound Vib, 2001, 246: 29–46
46 Liu G R, Nguyen-Thoi T, Lam K Y. An edge-based smoothed finite element method (ES-FEM) for static, free and forced vibration analyses of solids. J Sound Vib, 2009, 320: 1100–1130
47 Castellazzi G. On the performances of parametric finite elements when geometry distortions occur. Finite Elem Anal Des, 2011, 47: 1306–1314
48 Lee N S, Bathe K J. Effects of element distortions on the performance of isoparametric elements. Int J Numer Meth Eng, 1993, 36: 3553–3576
49 Tang X H, Zheng C, Wu S C, et al. A novel four-node quadrilateral element with continuous nodal stress. Appl Math Mech-Engl Ed, 2009, 30: 1519–1532
50 Parlett B N. The Symmetric Eigenvalue Problem. Upper Saddle River: Prentice-Hall, 1980
51 Zheng C, Tang X H, Zhang J H, et al. A novel mesh-free poly-cell Galerkin method. Acta Mech Sin, 2009, 25: 517–527